Journal of Building Engineering 71 (2023) 106441

Contents lists available at ScienceDirect

Journal of Building Engineering

journal homepage: www.elsevier.com/locate/jobe

Utilization of artificial interior stone sludge as fine aggregate in controlled low-strength material (CLSM)

Yoonjae Shin [a,1], Jeong Gook Jang [b,1], Jaesuk Choi [a], Goeun Jun [a], Chiyoung Park [c], G.M. Kim [d,**], Beomjoo Yang [a,*]

[a] School of Civil Engineering, Chungbuk National University, 1 Chungdae-ro, Seowon-gu, Cheongju, 28644, Republic of Korea
[b] Division of Architecture and Urban Design, Urban Science Institute, Incheon National University, 119 Academy-ro, Yeonsu-gu, Incheon, 22012, Republic of Korea
[c] Department of Energy Science and Engineering, Daegu Gyeongbuk Institute of Science and Technology, 333 Techno Jungang Daero, Hyeongpun-Eup, Daegu, Republic of Korea
[d] Korea Institute of Geoscience and Mineral Resources, 124 Gwahak-ro, Yuseong-gu, Daejeon, 34132, Republic of Korea

ARTICLE INFO

Keywords:
Artificial interior stone
Sludge
Fine aggregate
Controlled low-strength material
Predictions

ABSTRACT

Artificial interior stone, also known as imitation marble, is a representative high-end building interior material, the market share of which has been gradually increasing. Thus, the amount of waste sludge generated by its manufacture has also been rapidly increasing. However, because of a lack of a specific recycling plan, this waste is presently being disposed of in landfills. This study was conducted with the objective of recycling sludge into a fine aggregate for a controlled low-strength material (CLSM). The physicochemical properties of the sludge were investigated through various analyses. Subsequently, the material properties of sludge-containing CLSM in terms of compressive strength, bleeding rate, water absorption, and heavy metal content were examined. Through a combination of genetic algorithm-based machine learning and experimental results, a model equation that can predict the compressive strength of a CLSM specimen according to material composition was developed. This research presents a novel approach to recycling waste sludge from interior stone production as a fine aggregate for CLSM, addressing both environmental concerns and waste management in the industry.

1. Introduction

Interest in materials for building interiors has been increasing since people have been spending more time inside [1]. One high-end interior material is imitation marble, also referred to as artificial stone, cultured marble, and marbelite, among others. Imitation marble, which is composed mainly of natural quartz, is collectively referred to as engineered stone or artificial interior stone (AIS). Because AIS contains natural quartz, it is known to have a texture superior to those of acrylic-based products, and excellent chemical stability and scratch resistance [2]. AIS, which is currently being produced in large quantities at competitive prices, is widely applied in various parts of buildings, such as countertops, indoor walls, and floors [3].

A summary of the production process of AIS is as follows (Fig. 1): The size and color of the quartz powder intended by the

* Corresponding author.
** Corresponding author.
E-mail addresses: k.gm@kigam.re.kr (G.M. Kim), byang@cbnu.ac.kr (B. Yang).
[1] These authors contributed equally to this work.

https://doi.org/10.1016/j.jobe.2023.106441
Received 12 January 2023; Received in revised form 22 March 2023; Accepted 30 March 2023
Available online 5 April 2023

manufacturer are selected, and the powder is placed onto a formwork. A polymer film composed of unsaturated polyester (UPE) and styrene monomer is then applied to cover the surface (Fig. 1(a)). The initial product is manufactured with the application of an appropriate temperature and pressure (Fig. 1(b)). Finally, the material is cut and ground with the spraying of grinding water composed of water, polyvinyl alcohol (PVA), polyaluminum chloride (PAC), and calcium hydroxide to complete the final product.

During this manufacturing process, waste sludge mixed with moisture, quartz, and polymers is generated in large quantities. Currently, this large amount of waste is being buried entirely without an appropriate treatment method. Moreover, as the AIS market gradually grows, the amount of such sludge is expected to increase. Meanwhile, endeavors related to climate change and carbon neutrality, with aims of maximizing the recycling of waste and minimizing the consumption of resources, have been emerging worldwide. Therefore, in line with this cause, this study attempted to evaluate the potential of using AIS sludge as a substitute for typical fine aggregates.

The application of various wastes as constituents of construction materials has already been explored. For example, Katz and Kovler [4] applied various industrial by-products, such as kiln dust, asphalt dust, fly ash, coal bottom ash, and quarry waste, to the formulation of a controlled low-strength material (CLSM). It was demonstrated that CLSM with improved properties can be achieved through the simultaneous application of conventional pozzolanic admixtures and unreacted materials, such as asphalt dust and quarry waste [4]. Lee et al. [5] studied the properties of alkali-activated CLSM, excluding Portland cement. Three different industrial by-products (fly ash, slag, and bottom ash) were utilized as constituent materials for the CLSM, and various physical properties of fresh and cured CLSM were measured. They reported that the mechanical characteristics of the CLSM can be adjusted based on the chemical composition of the alkali activator.

Do et al. [6] conducted an experimental study on CLSM mixed with red-brown waste, the main component of which was iron oxide, generated during the aluminum refining process. The red-brown waste was mixed with gypsum, fly ash, and lime in various ratios, and the microstructure and physical/chemical characteristics of each specimen were analyzed. Xiao et al. [7] conducted a study on CLSM properties according to the pozzolanic reaction between waste glass powder and hydrated lime. Based on Gibbs free energy minimization, the ratio of waste glass powder to hydrated lime binder was studied, and it was determined that a ratio of waste glass powder/hydrated lime of 8:2 formed the largest calcium-silicate-hydrate gel. To date, several studies have been conducted on the formulation of CLSMs from various industrial wastes. However, research on the use of AIS waste remains limited.

This study was conducted with the objective of recycling AIS sludge through its application in construction materials. According to ACI-229R-99 [8], CLSM is defined as a cement-based slurry with a compressive strength of 8.3 MPa or lower at 28 days of age and is used mainly as backfill for excavated ground. Because CLSM is not applied as a structural element, it does not require high mechanical performance. In particular, a flow of 200–220 mm, bleeding rate of 3% or less, compressive strength of 0.3–2.1 MPa, and specific weight of approximately 1.3–2.32 g/cm^3 are required by a CLSM for filling a small cavity [9–11].

The present study introduces a novel approach to addressing the environmental concerns surrounding the waste generated during the production of AIS by evaluating the potential of using sludge as a substitute for typical fine aggregates in CLSM. Unlike previous research, this study specifically targets AIS waste, a relatively unexplored area. Through comprehensive analyses of the physicochemical properties of AIS sludge and the subsequent determination of an optimal CLSM mixing ratio with sludge replacement, the study aims to contribute to waste recycling and resource conservation efforts. Additionally, the study employs a machine learning-based genetic algorithm in conjunction with experimental results to establish a model equation capable of predicting the compressive strength of CLSM specimens according to their material composition, further enhancing the applicability and practicality of the findings.

Therefore, in this study, the replacement of fine aggregate in CLSM with AIS sludge was investigated. Specifically, this CLSM is to be

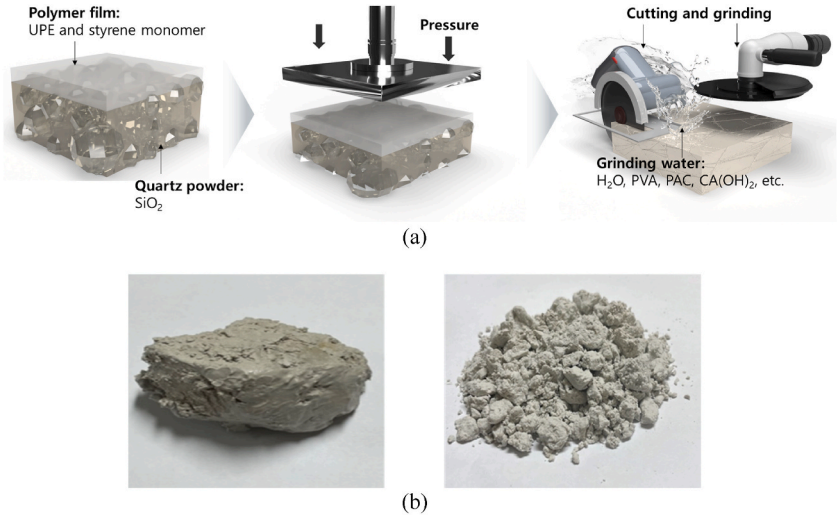

Fig. 1. (a) Manufacturing process of AIS and (b) wet and dry conditions of sludge by-product from the process.

used for filling small cavities. The physicochemical properties of the sludge were examined through moisture content analysis, particle size distribution analysis, field-emission scanning electron microscopy (FE-SEM), energy-dispersive X-ray spectrometry (EDS), X-ray diffraction (XRD), X-ray fluorescence (XRF), thermogravimetric analysis (TGA), and total concentration and leaching of heavy metal analyses.

Based on the analysis results, the CLSM mixing ratio was derived; specifically, the fine aggregate was replaced with sludge in various ratios. The compressive strength and specific weight of each specimen were measured on days 7, 14, and 28. The bleeding rate of the fresh specimen was also measured, and water absorption and total concentration/leaching of heavy metals were evaluated on the 28-day specimen. Subsequently, through a combination of the machine learning-based genetic algorithm (GA) and experimental results, a model equation that can predict the compressive strength of a CLSM specimen according to material composition was established.

2. Materials and methods

2.1. Characterization of AIS sludge

The sludge used in this study was generated during AIS production processes in a factory and was stored in an outdoor storage area without any specific treatment. The sludge was transported to the laboratory. To measure its moisture content, the initial weight of the wet sludge was first measured, and then the sludge was dried in an oven at 110 °C for 48 h. After the weight of the completely dried sludge was measured, its moisture content was calculated based on the ASTM C566-97 standard [12].

Subsequently, particle size distribution analysis of completely dried sludge powder was performed, using three randomly selected samples, and the average value was assumed to be the particle size of the entire sludge. The size distributions of the sludge particles were quantitatively analyzed using a laser diffraction particle size analyzer (HELOS H1483 & QUIXEL, Sympatec). Additionally, FE-SEM analysis was performed to obtain microscopic images of the sludge (LEO-1530, ZEISS). EDS analysis was also performed to identify the sludge constituents and their distribution.

The XRD pattern of the sludge was collected based on scans of the samples on a rotating stage at 5–65° 2θ using a JP/SmartLab (Rigaku Co.). XRF analysis was also performed to determine the chemical composition and crystal structure of the sludge (ZSX Primus 2, Rigaku Co.). TGA was performed using a TG 209 F1 instrument (NETZSCH Co., Ltd.). A sludge sample of 5–6 mg was used for the analysis, and the temperature was measured at a rate of 10 °C/min. To prevent oxidation of the specimen during the analysis process, nitrogen gas was introduced into the furnace of the equipment. In this TGA, relative weight variations were measured in the temperature range 25–950 °C. Finally, to evaluate the environmental impact of the sludge, total heavy metal concentration and leaching tests were conducted (ICP-OES Spectroblue, SPECTRO Co. Ltd).

2.2. CLSM specimen

2.2.1. Specimen formulations and fabrication procedure

Table 1 presents the formulation of the CLSM specimen, in which the fine aggregates were partially or entirely replaced with sludge. Herein, the sludge replacement rate for the fine aggregate was set as the experimental variable and was also used in the specimen names. For example, S30 denotes a CLSM specimen in which 30 wt% of the total fine aggregate is replaced with AIS sludge.

AIS sludge inevitably acquires moisture during the production process, the amount of which depends on the process time and place. Therefore, in this study, the flow of each specimen was fixed at 200 ± 5 mm [13], and the amount of water is listed in Table 1. The moisture content values of randomly selected sludge samples were then measured, as shown in Table 2, and the amounts of water including the average moisture content value of the sludge (27.45 ± 0.39%) are indicated in an additional column in Table 1.

In conventional mixtures, typically only the amount of water used in the production of the specimen is displayed. However, in this study, it was found that the sludge contains an average of 27.45% moisture, which is considered a substantial amount. We believed that the total amount of water incorporated into the specimen would have a significant impact on material performance, and accordingly, the total water content is also presented in Table 1. In other words, “Water with sludge moisture” in Table 1 can be considered as the actual total amount of water used in the fabrication of the CLSM specimens.

Type I ordinary Portland cement (OPC) (Sungshin Cement Co., Ltd.; specific gravity: 3.10–3.15) and fly ash (Hadong thermal power plant operated by Korea Southern Power Co., Ltd.; specific gravity: 2.35–2.45) were used as binder materials. Fine aggregate (Jumunjin Gyusa Co., Ltd.; specific gravity: 2.60–2.70) was also utilized in the experiment.

The mixture of OPC, fly ash, fine aggregate, and sludge was dry-mixed for 5 min using a mortar pan mixer. Subsequently, the mortar mixture was mixed further with water for 10 min. The mixture was cast into 50 mm^3 molds and wrapped to prevent moisture evaporation. The specimens were cured at 18–25 °C for 24 h and then demolded. Subsequently, the specimens were individually

Table 1
Mixture proportions of CLSM specimens expressed in weight ratios.

Specimens*	Cement	Type F fly ash	Sludge	Fine aggregate	Water	Water with sludge moisture	Target flow (mm)
S0	100	275	–	3100	760	760	200 ± 5
S30	100	275	930	2170	326	577	
S50	100	275	1550	1550	282	701	
S70	100	275	2170	930	326	912	
S100	100	275	3100	–	260	1097	

* Note that the digits included in the specimen names denote their sludge ratios (wt.%).

Table 2
Average moisture content of sludge (%).

Sludge	Before drying (g)	After 48 h of drying (g)	Moisture content (%)
1	71.85	52.49	26.95
2	64.11	46.48	27.50
3	84.05	61.54	26.78
4	66.78	47.96	28.18
5	94.90	68.37	27.96
6	78.86	57.30	27.34
7	82.06	59.54	27.44
8	105.22	76.43	27.36
9	113.22	82.18	27.42
10	97.82	70.81	27.61
Avg.			27.45

wrapped and further cured at the same temperature for 7, 21, and 28 days.

2.2.2. Characterization of CLSM specimen

The compressive strengths of the CLSM specimens cured for 7, 14, and 28 days were evaluated according to ASTM C109/C109M − 20 [14]. A universal testing machine (UTM) with a specification of 300 kN (RT-M-003-30PC, Ramt Co., Ltd.) was used for the evaluation, and a load was applied at a crosshead speed of 0.6 mm/min. The specific weight was calculated by dividing the weight of the specimen cured for 7, 14, and 28 days by the volume, in accordance with ASTM D1556 [15].

The bleeding characteristics of the CLSM specimens were evaluated in accordance with ASTM C232/C232M − 21 [16]. A 1000 mL cylinder was filled with 800 mL fresh mortar mixed within 3 min, and the cylinder was sealed to prevent water evaporation. After 3 and 20 h, the rate of bleeding was calculated using Eq. (1).

$$\text{Rate of bleeding } (\%) = \frac{V_w}{V_1} \times 100, \tag{1}$$

where V_W (mL) is the amount of water eluted after each duration (3 and 20 h). The variable V_W signifies the volumetric quantification of the excess water rising to the CLSM specimen's surface after 3 and 20 h. After the designated settling period has elapsed, the water accumulation on the surface can be visually assessed, and the water can be extracted utilizing a pipette or syringe. V_1 (mL) is the volume of the mortar, which was initially 800 mL.

The water absorption rate was determined in accordance with ASTM C1403-13 [17]. First, the initial weight of the 50 mm^3 specimen (W_0) was measured with an accuracy of 0.1 g. Afterward, supports that do not rust, expand, or contract were placed in a container, and specimens were set on the support. The container was filled with water (24 ± 8 °C) to submerge the specimen by 3.0 ± 0.5 mm from the bottom surface of the specimen and was covered to minimize evaporation. In the first 1–5 min, which is the initial absorption phase, sufficient water was added to maintain the original level. Subsequently, the weight of each specimen was measured at 0.25, 1, 4, and 24 h. The water absorption rate was calculated using Eq. (2).

$$\text{Rate the water absorption } (\%) = (W_t - W_0) \times \frac{L_1 \cdot L_2}{10000}, \tag{2}$$

where W_T denotes the weight of the specimen after the specified duration (0.25, 1, 4, and 24 h) (g); W_0 is the initial weight of the specimen (g); and L_1 and L_2 denote the average length and width of the specimen (mm), respectively.

To evaluate the environmental impact of the hydrated CLSM specimens, the total concentrations and leaching of heavy metals were analyzed. CLSM specimens cured for 28 days were ground into powder and analyzed for the presence of heavy metals lead (Pb), chromium (Cr), copper (Cu), and cadmium (Cd) using ICP-OES Spectroblue (SPECTRO Co. Ltd).

2.3. GA-based model

Experimentation is widely accepted as the predominant method for validating the mixture and performance of construction materials. This is because the theoretical interpretation of the complex chemistry involved in hydration, which takes about 28 days, is relatively challenging and inefficient. Machine learning technology has been rapidly developing and is increasingly being employed in diverse fields, with its rate of application predicted to continue rising.

Therefore, a genetic programming toolbox for the identification of physical systems (GPTIPS) was used to predict the mechanical properties of the sludge-containing CLSM specimens. GPTIPS is an open-source programming and symbolic machine-learning platform that runs in a MATLAB environment [18]. Based on experimental results, it generates a quantitative structure–activity relationship (QSAR) model [19–21]. The multigene symbolic regression algorithm, which is the main principle for the present numerical analysis, has been applied in various fields, and its capabilities have been demonstrated [22–24].

AIS sludge is an industrial waste that has been rapidly generated in recent years; however, research on its application in construction materials remains incomplete. Therefore, it was expected that the combination of the existing models and the experimental data obtained in this study would have limitations in the prediction [25–27]. To address this, a symbolic model formula for predicting the material performance was derived based on machine learning. Based on the mixture formulation of the CLSM specimen, the input

variables were set to cement, fly ash, sludge, fine aggregate, and water, and the output was set to compressive strength [28,29]. The algorithm configuration and driving principle for the GPTIPS are described in more detail in literature [22–24,30–32].

3. Results and discussion

3.1. Sludge characterization

Fig. 2 shows the results of particle size distribution analysis for the sludge and OPC. The cumulative distributions of the particles are shown in Fig. 2(a), and the density distributions of the particles are shown in Fig. 2(b). The sludge had a particle size of approximately 5–10 μm, which was analyzed to have a distribution of $D_{10} = 1.17$ μm, $D_{50} = 4.93$ μm, and $D_{90} = 16.08$ μm. For comparison, OPC had a particle size of approximately 25–50 μm, which was analyzed to have a distribution of $D_{10} = 9.83$ μm, $D_{50} = 18.0$ μm, and $D_{90} = 51.91$ μm. From the analysis, it was confirmed that the particle size of the sludge was smaller than that of the OPC. This suggested that the incorporation of sludge would effectively fill the small voids inside the CLSM.

The results of FE-SEM analysis on the sludge are shown in Fig. 3. The shape of the sludge was irregular, and there were some large particles (20–70 μm) among the fine particles, estimated to be 5 μm on average. In general, spherical particles are preferred as fine aggregates for the sake of fluidity; however, it was difficult to find spherical particles in the sludge. Based on the particle size and shape, it is expected that the sludge particles would not help, or may even decrease the fluidity because of interlocking between the particles [33,34]. Therefore, in this study, to obtain the target flow, the unit amount of water was varied according to the sludge replacement rate. Meanwhile, the elemental components of the sludge were analyzed via EDS, and the results are presented in Fig. 4. It shows the mapping of the distribution of C, O, and Si in the sludge and the individual distributions of each element.

XRD and XRF analyses were performed to determine the chemical properties of the AIS sludge. As shown in Fig. 5, the crystalline peaks observed on the sludge exhibited diffuse peaks over an angular range of 10–35°, indicating that most of the sludge consisted of quartz. The hexagonal silica phase of quartz is classified under space group P3121 (space group number: 152), and a similar pattern was indexed in this XRD analysis [35]. By contrast, the small amount of polymer used for AIS production was not indexed in the XRD pattern; therefore, it is inferred that the AIS used here mostly consisted of quartz. The chemical and mineral compositions of the sludge, as measured by XRF analysis, are presented in Table 3. For comparison, the table also includes the XRF data for the cement used in this experiment, as provided by the manufacturer. The data indicate that the sludge consisted mainly of SiO_2 (97.5 wt%) with various

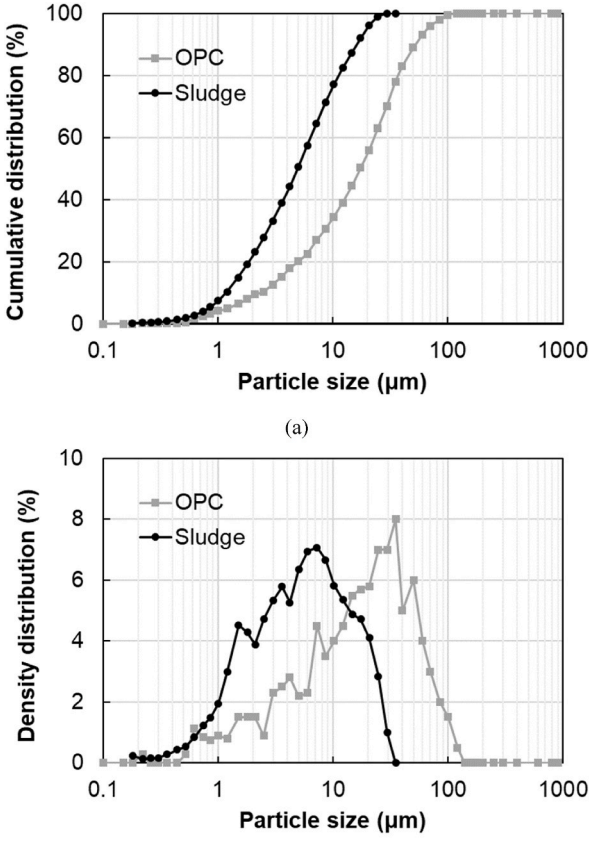

Fig. 2. Particle size distribution of sludge and OPC: (a) Cumulative distribution and (b) density distribution.

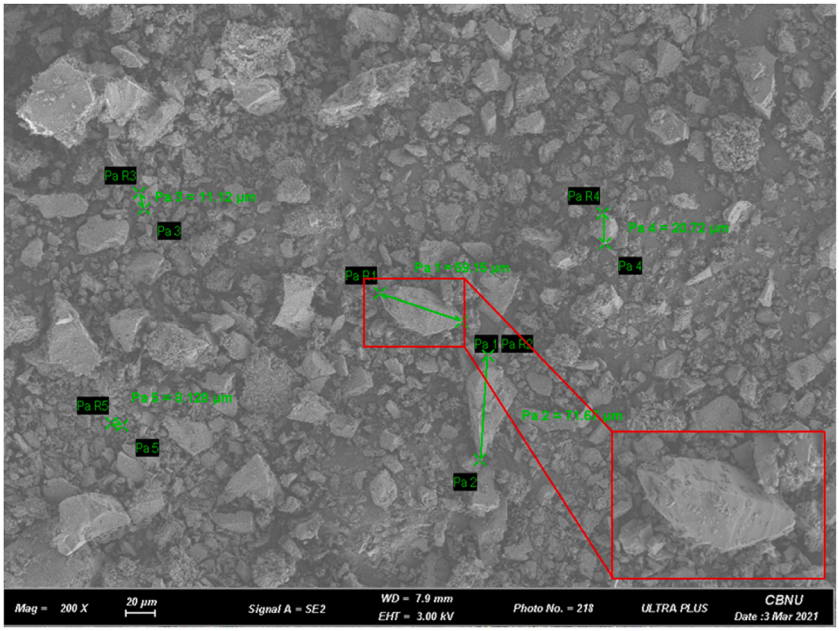

Fig. 3. FE-SEM images of sludge particle.

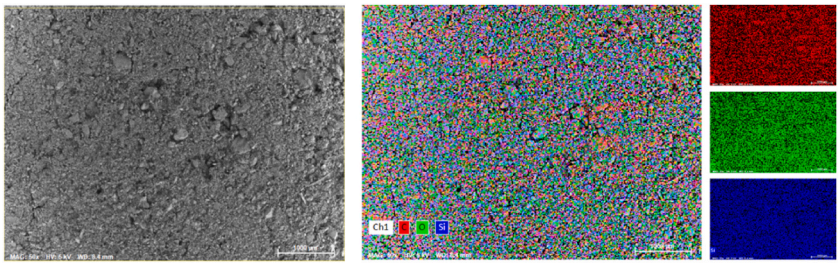

Fig. 4. EDS mappings for elements C, O, and Si.

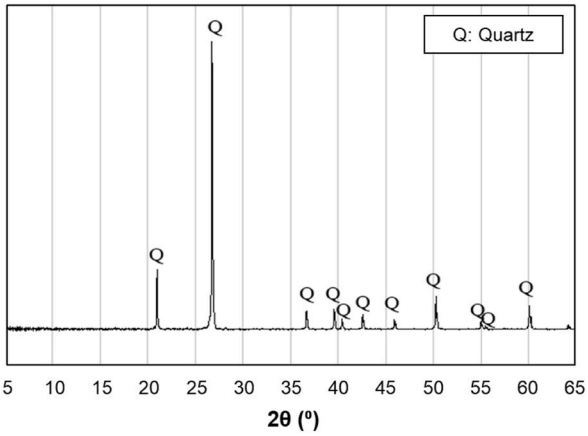

Fig. 5. XRD pattern of AIS sludge powder.

minor composites (Al_2O_3, CaO, and Fe_2O_3).

The TG/DTG results for the sludge are presented in Fig. 6. It can be observed that weight loss occurred at approximately 100 °C and then decreased by approximately 10% from 200 °C to 400 °C. It is inferred that the weight loss that occurred near 50–150 °C was due to

Table 3
Chemical compositions of cement and sludge.

X-ray fluorescence (wt.%)		
	Cement	Sludge
SiO_2	20.4	97.5
Al_2O_3	4.6	0.7
CaO	60.3	0.4
Fe_2O_3	3.2	0.3
MgO	3.3	–
TiO_2	0.3	0.6
SO_3	2.3	–
Mn_2O_3	0.1	–
P_2O_5	0.1	–
SrO	0.1	–
Na_2O	0.2	–
K_2O	0.9	0.1
ZrO_2	–	–

the evaporation of the water contained in the sludge [36]. The sludge used for TGA was dried at 110 °C for more than 48 h; however, Si–OH groups could be formed because of the hydrophilicity of SiO_2 [37]. Furthermore, as shown in Fig. 2, approximately 10% of the sludge was composed of submicron particles (≤1 μm). Thus, an increase in the specific surface area due to reductions in the particle size could be favorable for attracting free water on the surfaces of the submicron particles [38,39]. Specifically, physically bound water on the surfaces of the submicron particles could be evaporated in the temperature range.

It is also inferred that the weight loss that occurred in the range 200–400 °C was due to the decomposition of small amounts of polymer and organic carbon [40]. The decomposition and carbonization temperature ranges of UPE, PVA, and PAC, which are the polymers utilized in the production process of AIS, are 130–400 °C [41], 200–450 °C [42], and 150–200 °C [43], respectively. It is believed that the decomposition features contributed to the thermal mass loss in the TGA. Beyond 400 °C, the weight did not exhibit any significant changes until 950 °C. This is due to the much higher decomposition temperature of SiO_2, which is the main component of the sludge. It is known that at atmospheric pressure conditions, SiO_2 maintains a stable quartz phase below approximately 600 °C [44–46].

To evaluate the environmental impact of the sludge, the total concentration and leaching of heavy metals from the sludge were analyzed (Table 4). The heavy metals considered in this study were Pb, Cr, Cu, and Cd, and their inclusions in the sludge were analyzed. With regard to the total concentrations, those of Pb and Cd, as indicated by "<30.0" in the table, were smaller than the minimum concentration that the equipment can measure. By contrast, those of Cr and Cu, which were present in relatively large amounts compared with Pb and Cd, were approximately 0.0032 wt% and 0.0009 wt%, respectively, in terms of weight ratio. Therefore, it can be concluded that the two heavy metals (Cr and Cu) were also present in trace amounts. The results of the leaching tests on the sludge are presented in Table 4. Notably, the total concentration is the result of dissolving entire samples of the sludge in acid, whereas the leaching test measures the amounts of heavy metals eluted from the sludge. All heavy metal elution values for the sludge were analyzed to be "non-detectable (ND)," indicating that there will be no environmental problem if the sludge is used as a construction material and recycled fine aggregate.

3.2. *Effects of AIS sludge on CLSM*

Fig. 7 shows the compressive strengths of the CLSM specimens at 7, 14, and 28 days according to the sludge replacement ratio for the fine aggregate. In all cases, the compressive strengths of the specimens that included sludge (S30, S50, S70, and S100) were measured to be higher than that of S0. For the same target flow condition of 200 ± 5 mm, the 28-day compressive strengths of the

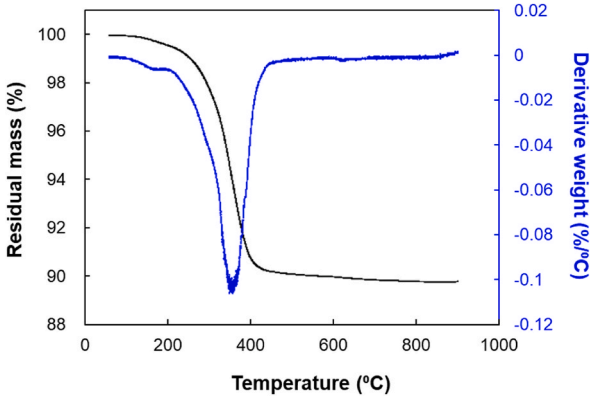

Fig. 6. Thermal analysis results of sludge.

Table 4
Total concentration and leaching of heavy metals from sludge.

Measure	Ingredient (mg/kg)			
	Pb	Cr	Cu	Cd
Total concentration	<30.0	31.7	9.18	<30.0
Leaching test	ND	ND	ND	ND

*ND: Not detected.

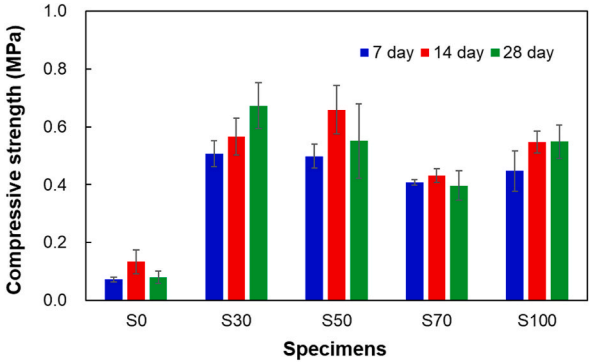

Fig. 7. Compressive strengths of CLSM specimens with varying sludge replacement ratios and curing days.

specimens in which 30 and 50 wt% of the fine aggregates were replaced by the sludge were 0.67 and 0.55 MPa, respectively. This is an increase of approximately 8.5 times compared to that of S0. Overall, the compressive strength of the S50 specimen was the highest, and gradually decreased as more sludge was added.

The differences in the compressive strength according to the sludge replacement rate mostly matched the trend for the incorporated total water with sludge moisture. Specifically, as the total amount of water increased, the compressive strength decreased. This indicated that the incorporated water had a significant effect on the compressive strengths of the CLSM specimens. Interestingly, the compressive strengths of S70 and S100 were higher than that of S0, although there was also more water than in S0 because of sludge replacement. It is inferred that the submicron-sized sludge particles, which are smaller than cement and fine aggregate, contributed to reductions in large pores that acted as defect sites [47,48]. Evenly dispersed sludge particles smaller than fine aggregates resulted in an improvement in strength while filling large pores in the CLSM specimens [49]. In addition, given the amount of mixed water, the compressive strengths of specimens S30 and S50 were high. This phenomenon can be attributed to the effective filling of micropores in the specimens and the reduction of water content required to maintain a similar flow value when sludge with an average particle size of 5 μm replaced 30 and 50 wt% of fine aggregates. In other words, the filling effect of the sludge and the reduction of water content can simultaneously influence the compressive strength of both S30 and S50.

SiO_2, which constitutes most of the sludge, exhibits strong hydrophilicity and may have attracted many water molecules. Thus, the water molecules, forming large pores during the hydration process, were uniformly dispersed by the sludge incorporated into the CLSM. Consequently, it induced the formation of relatively even and small pores inside the specimen [50]. By contrast, in the S0 specimen without the sludge, the free-water effect was dominant. This caused an increase in the formation of relatively large pores, resulting in defect sites, and consequently, a relatively low compressive strength. In conclusion, appropriate sludge replacement of fine aggregates (30–50 wt%) reduces the porosity of the material and the quantity of more harmful pores, contributing to a higher

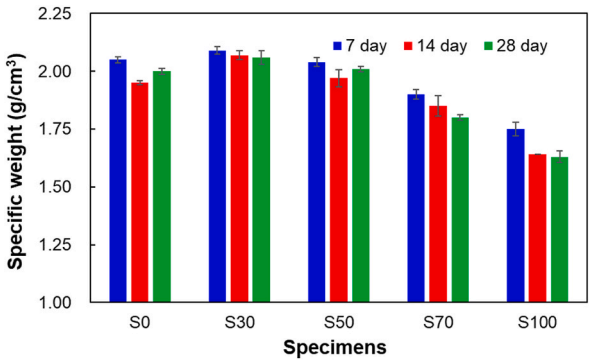

Fig. 8. Specific weights of CLSM specimens with varying sludge replacement ratios and curing days.

compressive strength [51].

Fig. 8 shows the specific weight of each specimen. The specific weights of S30 and S50 did not significantly differ from that of S0. However, in the case of S70 and S100, in which 70 and 100 wt% of the fine aggregates were substituted with sludge, the specific weights gradually decreased. It is inferred that the sludge, which had more water than the fine aggregate, caused greater evaporation of water over time. In addition, the specific gravity of the sludge (2.7), which was lighter than that of fine aggregate (3.1), contributed to weight reductions in the specimens. It should be noted that the abovementioned discussions are difficult to prove quantitatively, and the conclusions drawn are based on the results of the experiment. Further analysis is necessary for a more precise examination, but it is considered a limitation of this research.

Fig. 9 shows the range of compressive strength and density recommended by the ACI 229 Committee for CLSMs used in the filling of small cavities [9–11]. Additionally, previously published CLSM research results [4,9,10,52,53] are presented in addition to the present experimental data. As shown in Fig. 9, both the compressive strength and density were found to be within the recommended ranges. However, the measured compressive strength was lower than the experimental results obtained by other groups [4,10,52] for the same density.

Table 5 shows the bleeding characteristics of the sludge-containing CLSM specimens. Bleeding refers to the accumulation of water at the top of a specimen in an unconsolidated state [36]. The bleeding rates after 3 h were 0.06, 0.02, 0.11, and 0.02%, respectively, and the final values were all measured to be less than 0.001%. This value is significantly lower than the standard recommended by the committee (<3), and therefore, it was concluded that the effect of bleeding was insignificant for most sludge-containing specimens. As stated previously, the sludge is composed mainly of hydrophilic SiO_2, which has a relatively large specific surface area compared to those of fine aggregates. Consequently, a large number of water molecules attach to their surfaces [54]. It is inferred that the physicochemical properties of the sludge contributed to reductions in the bleeding rate, as listed in Table 6.

It is worth noting that the amount of mixing water used in specimen S70 was the second highest among all specimens. In addition, 70% of the aggregate was replaced with sludge in S70, which introduced a significant amount of moisture contained in the sludge into the mixture. As a result, S70 had the second highest amount of total water used in the mixture after S100. It is presumed that a relatively large amount of total water and the combination of aggregate and sludge were appropriately matched, resulting in a somewhat larger amount of bleeding compared to other specimens. In S100, although the largest amount of water was applied to the mixture, it is considered that the relatively small particle size of the sludge contributed to reducing the amount of bleeding.

Fig. 10 presents the water absorption test results for the CLSM specimens. Evidently, except for the initial 1 h, the overall absorption rate increased as the replacement rate of the sludge increased. For all specimens, it was observed that the specimens with sludge (S30–S100) absorbed greater amounts of water than that absorbed by S0. This was because the amount of water required for the fixed target flow (200 ± 5 mm) was already fulfilled by the moisture contained in the sludge. This suggests that an increase in the total amount of water causes deformation of the internal pore properties, thereby increasing the water absorption rate of the specimen. Herein, the discussions are the inference based on the mixing ratio and absorption rate results, and further analysis is required for a quantitative understanding of the mechanism. In this study, it was practically challenging to quantitatively analyze the mechanisms related to this phenomenon across all ranges, which can be considered a limitation of the research.

To evaluate the environmental impact of CLSM, total heavy metal concentration and leaching tests for Pb, Cr, Cu, and Cd in the specimens were conducted. The purpose of this analysis was to examine whether heavy metals are generated during the hydration period. Therefore, only the S50 and S100 specimens, in which the sludge was replaced with 50 and 100 wt% of fine aggregate, were considered. In the analysis of the total concentrations of heavy metals, small amounts of Cr and Cu were detected; however, Cr and Cu were observed to be the highest in S0 and lower in S50 and S100. This suggests that the Cr and Cu detected in the analysis are contained mainly in the OPC or fine aggregate. In the case of Cr and Cu in S0, in which the highest amounts were detected, the concentrations were approximately 0.029 and 0.006 wt%, respectively, which are insignificant. Notably, the total concentrations of heavy metals were derived based on analyses of the material after complete dissolution in acid, and thus it is unlikely to occur in normal environmental conditions. Moreover, with regard to the heavy metal leaching test, which involves conditions that may occur in a normal

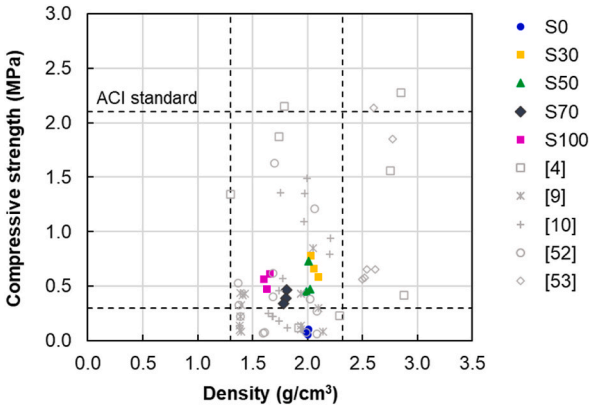

Fig. 9. Specific weight-compressive strength results of the present study with design code (ACI-229R-99) and references [4,9,10,52,53].

Table 5
Bleeding rates of CLSM specimens formulated via replacement of aggregate with sludge.

	Bleeding rate (%)			
	S30	S50	S70	S100
3 h	0.06	0.02	0.11	0.02
24 h	<0.001			

Table 6
Total concentrations and leaching of heavy metals from sludge-containing specimens.

Measure	Specimens[a]	Ingredient (mg/kg)			
		Pb	Cr	Cu	Cr
Total concentration	S0	ND	63	290	ND
	S50	ND	ND	110	ND
	S100	ND	ND	80	ND
Leaching test	S0	ND	ND	ND	ND
	S50	ND	ND	ND	ND
	S100	ND	ND	ND	ND

[a] ND: Not detected.

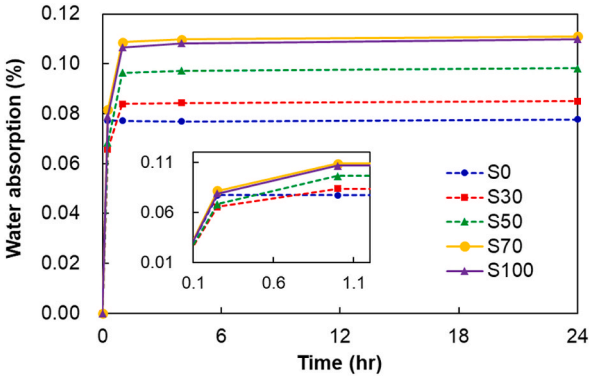

Fig. 10. Results of water absorption test on CLSM specimens (%).

environment, no heavy metals were detected in any specimen.

3.3. Experimental comparisons

The experimental results obtained in the present study were applied to the GPTIPS algorithm, and the compressive strength model formula for CLSM mixed with sludge was derived as follows:

$$\sigma_{comp} = \cos(S + \exp(S)) + 1.7\sin(S + \sin(S)) - 0.05\sin\left(\sqrt{d}\right) - 0.15W\cos(S) - 0.2, \quad (3)$$

where σ_{comp} signifies the compressive strength of the 28-day CLSM (MPa), d is the curing period (days), and S and W denote the ratios of sludge-to-aggregate (s/a) and water-to-binder (w/b), respectively. Fig. 11 shows a comparison between the derived model equation and actual experimental results. The R-squared (R^2) value in Fig. 11 is 0.864, which indicates a relatively high accuracy considering the limited experimental data.

3.4. Model validation

To evaluate the validity of the derived model, parametric studies with varying input values were performed, and the results are presented in Fig. 12(a)-(c) Fig. 12(a) illustrates the impact of sludge content on the compressive strength of CLSM. In this case, the curing period and the water-to-binder ratio (w/b; W) were fixed at 28 days and 0.8, respectively. The proposed model was used to predict the effects of varying the sludge-to-aggregate ratio (s/a; S) from 0 to 0.3, 0.5, 0.8, and 1. A ratio of 0 represents a specimen without any sludge, while 1 denotes a CLSM specimen where all fine aggregates have been replaced with sludge. In line with the actual experimental results, specimens with sludge substituting for fine aggregates exhibited higher compressive strengths than those without. However, as the replacement rate of fine aggregates increased, the compressive strength gradually decreased. This nonlinear prediction outcome is believed to be due to the data-driven model derived from the experiments conducted in this study.

Fig. 12(b) depicts the predicted effects of the W on the compressive strength of CLSM. The curing period was fixed at 28 days, and

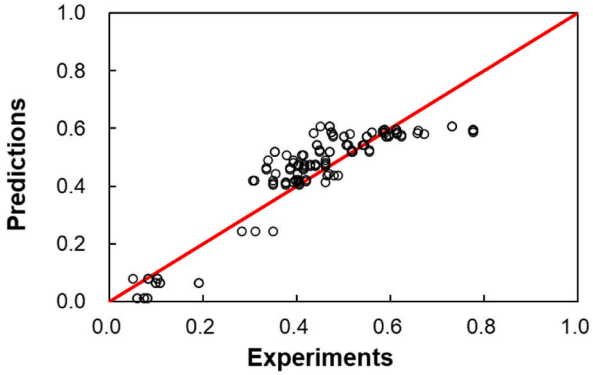

Fig. 11. Correlation between predicted values and experimental results ($R^2 = 0.864$).

the S was set at 0.5. The model predicted the changes in CLSM compressive strength as W increased from 0.3 to 2. In accordance with the mechanism analysis from the experiments, the amount of water had a significant impact on the compressive strength of CLSM. In other words, it was identified as the variable with the most significant influence on the compressive strength value in the data-driven model. Fig. 12(c) presents the predicted changes in CLSM compressive strength based on the curing period. Both W and S were fixed at 0.8 and 0.5, respectively, and the curing period was varied from 1 to 28 days. The curing period was found to have a negligible influence on the compressive strength of the specimens, which somewhat deviates from the actual experimental results. This discrepancy can be attributed to the insufficient amount of data regarding the absolute values of the curing period. Since the experiments only had three variables, 3, 7, and 28 days, the model could not accurately predict the outcomes based on the changes in the curing period. This limitation, resulting from the insufficiency of data variables, should be addressed in future research.

4. Conclusions

This paper presents a study on the formulation and evaluation of CLSM in which fine aggregates were replaced with AIS sludge. Various analyses were performed on the sludge to investigate its moisture content, particle size distribution, morphological characteristics, chemical composition, thermal properties, and heavy metal content. The mixing ratio of sludge-containing CLSM, in which the fine aggregate was replaced in various ratios, was derived, and the material performance was evaluated. The flow of the CLSM specimen was set at 200 mm, and tests were performed on the compressive strength, specific weight, bleeding rate, water absorption, total concentration, and leaching of heavy metals from the specimen. Finally, through an application of the GPTIPS algorithm based on the experimental results, a compressive strength prediction model for the CLSM specimen according to the formulation was derived.

- In terms of chemical composition, most of the sludge is composed of SiO_2 and contains almost no heavy metals. Specifically, the heavy metals analysis was conducted through total concentration and leaching tests of Pb, Cr, Cu, and Cr elements in both the sludge raw material and CLSM specimens with sludge incorporated. In the case of heavy metal total concentration analysis, it was revealed that approximately 9–32 mg/kg were present, which is a very low value. Importantly, no detection was observed in the leaching tests, which could directly pose environmental concerns. The amounts of various polymers applied during AIS preparation also remained very low.
- The compressive strength of the CLSM specimen, in which fine aggregates were replaced with the sludge, was improved compared to that of the specimen without sludge. The optimal displacement ratio of the sludge was determined to be 30–50 wt%. The majority of the performance improvement through the use of sludge is believed to be due to the smaller particle size compared to conventional fine aggregates and cement particles. The filling of voids within the material by the average particle size of around 5 μm and the additional hydration of sub-micron particles smaller than 500 nm are expected to have resulted in a more densely packed structure within the specimen.
- The flow, bleeding, compressive strength, and density values of the CLSM, including the sludge, were within the performance ranges recommended by ACI-229R-99. For all specimens, the flow was 200±5 mm, and bleeding was less than 0.001% after 24 h, satisfying the required conditions. Moreover, the average compressive strength for S30–S100 was 0.521 MPa, meeting the standard requirement of 0.3–2.1 MPa. The average density of the S30–S100 specimens was 1.84 g/cm^3, which also fell within the standard range of 1.3–2.32 g/cm^3.
- Based on the experimental results, a GA-based model formula was developed, and its accuracy was approximately $R^2 = 0.864$. The variables considered in the model were the sludge-to-fine aggregate substitution rate, the water-to-binder ratio, and the curing period. Within the range of the considered variables in the experiment, it was confirmed that the model accurately simulates even the non-linear characteristics. The most influential factor in the data analysis was found to be the water-to-binder ratio, and ultimately, the amount of water used in specimen fabrication had the greatest impact on the compressive strength of the specimens. This finding was consistent with the experimental analysis results.

The measured compressive strength was lower than the experimental results reported in literature. This is a limitation of the present study and should be addressed through the use of additional admixtures or method modifications. In addition, the derived

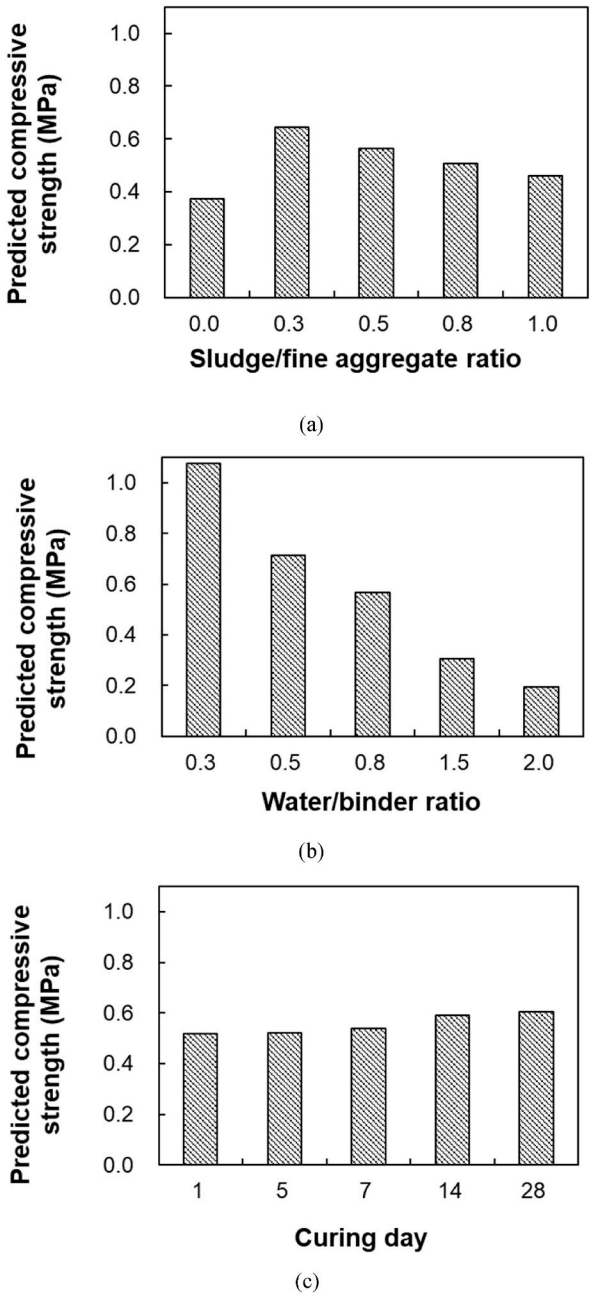

Fig. 12. Model-based parametric studies with respect to (a) sludge replacement ratio and (b) water/binder ratio, and (c) curing day of CLSM specimen.

model was based on limited experimental results, and additional data and modification of algorithms are necessary. We intend to focus on this aspect in future research.

Credit author statement

Yoonjae Shin: Writing – original draft, Conceptualization, Methodology; **Jeong Gook Jang**: Data curation, Investigation; **Jaesuk Choi**: Data curation; **Goeun Jun**: Conceptualization, Methodology; **Chiyoung Park**: Validation, Formal analysis; **G. M. Kim**: Writing – review and editing; **Beomjoo Yang**: Writing – review and editing, Supervision.

Declaration of competing interest

The authors declare that they have no known competing financial interests or personal relationships that could have appeared to

influence the work reported in this paper.

Data availability

No data was used for the research described in the article.

Acknowledgments

This work was supported by a National Research Foundation of Korea (NRF) grant funded by the Korean government (MSIT) (2020R1C1C1005063 and 2022R1A4A3029737) and by the Industrial Strategic technology development program-Development of manufacturing technology of hardened cement with carbonation curing (RS-2022-00155662, Development of manufacturing and application technology of 1,000 ton/year class hardened cement with carbonation curing) funded by the Ministry of Trade, Industry & Energy (MOTIE, Korea).

References

[1] S. Nundy, A. Ghosh, A. Mesloub, G.A. Albaqawy, M.M. Alnaim, Impact of COVID-19 pandemic on socio-economic, energy-environment and transport sector globally and sustainable development goal (SDG), J. Clean. Prod. 312 (2021), 127705.
[2] R. Bugini, C. Corti, L. Folli, L. Rampazzi, The use of mortars to imitate white marble and other stones, Int. J. Conserv. Sci. 9 (1) (2018) 3–12.
[3] H. Rix, S. Emmitt, Imitative material culture: towards a philosophy for the authentic conservation of historical artificial materials and imitative techniques, J. Architect. Conserv. 28 (1) (2022) 1–21.
[4] A. Katz, K. Kovler, Utilization of industrial by-products for the production of controlled low strength materials (CLSM), Waste Manag. 24 (5) (2004) 501–512.
[5] N.K. Lee, H.K. Kim, I. Park, H.K. Lee, Alkali-activated, cementless, controlled low-strength materials (CLSM) utilizing industrial by-products, Construct. Build. Mater. 49 (2013) 738–746.
[6] T.M. Do, G.-O. Kang, Y.-s. Kim, Development of a new cementless binder for controlled low strength material (CLSM) using entirely by-products, Construct. Build. Mater. 206 (2019) 576–589.
[7] R. Xiao, P. Polaczyk, X. Jiang, M. Zhang, Y. Wang, B. Huang, Cementless controlled low-strength material (CLSM) based on waste glass powder and hydrated lime: synthesis, characterization and thermodynamic simulation, Construct. Build. Mater. 275 (2021), 122157.
[8] ACI, Controlled Low-Strength Materials, American Concrete Institute, 1999. ACI-229R-99.
[9] R. Taha, A. Alnuaimi, K. Al-Jabri, A. Al-Harthy, Evaluation of controlled low strength materials containing industrial by-products, Build. Environ. 42 (9) (2007) 3366–3372.
[10] L. Du, K.J. Folliard, D. Trejo, Effects of constituent materials and quantities on water demand and compressive strength of controlled low-strength material, J. Mater. Civ. Eng. 14 (6) (2002) 485–495.
[11] W.S. Adaska, Controlled low-strength materials, Concr. Int. 19 (4) (1997) 41–43.
[12] ASTM, Standard Test Method for Total Evaporable Moisture Content of Aggregate by Drying, American Society for Testing and Materials International, 2017. ASTM C566-97.
[13] S. Kourounis, S. Tsivilis, P. Tsakiridis, G. Papadimitriou, Z. Tsibouki, Properties and hydration of blended cements with steelmaking slag, Cement Concr. Res. 37 (6) (2007) 815–822.
[14] ASTM, Standard Test Method for Compressive Strength of Hydraulic Cement Mortars, American Society for Testing and Materials International, 2020. ASTM-C109/C109M-20.
[15] ASTM, Standard Test Method for Density and Unit Weight of Soil in Place by the Sand-Cone Method, ASTM D1556 American Society for Testing and Materials International, 2016.
[16] ASTM, Standard Test Method for Bleeding of Concrete, American Society for Testing and Materials International, 2021. ASTM C232/C232M-21.
[17] ASTM, Standard Test Method for Rate of Water Absorption of Masonry Mortars, American Society for Testing and Materials International, 2015. ASTM C1403-13.
[18] D.P. Searson, D.E. Leahy, M.J. Willis, GPTIPS: an open source genetic programming toolbox for multigene symbolic regression, in: Proceedings of the International Multiconference of Engineers and Computer Scientists, Citeseer, 2010, pp. 77–80.
[19] J. Nuñez, M. Cruchaga, G. Tampier, Wave analysis based on genetic algorithms using data collected from laboratories at different scales, Eur. J. Mech. B Fluid 95 (2022) 231–239.
[20] D.P. Searson, D.E. Leahy, M.J. Willis, Predicting the Toxicity of Chemical Compounds Using GPTIPS: a Free Genetic Programming Toolbox for MATLAB, Intelligent Control and Computer Engineering, Springer, 2011, pp. 83–93.
[21] K. Miladirad, E.M. Golafshani, M. Safehian, A. Sarkar, Modeling the mechanical properties of rubberized concrete using machine learning methods, Comput. Concr. 28 (6) (2021) 567–583.
[22] C. Hii, D.P. Searson, M.J. Willis, Evolving toxicity models using multigene symbolic regression and multiple objectives, International Journal of Machine Learning and Computing 1 (1) (2011) 30.
[23] Y. Shin, H.M. Park, J. Park, H. Cho, S.-E. Oh, S.-Y. Chung, B. Yang, Effect of polymer binder on the mechanical and microstructural properties of pervious pavement materials, Construct. Build. Mater. 325 (2022), 126209.
[24] J. Žegklitz, P. Pošík, Benchmarking state-of-the-art symbolic regression algorithms, Genet. Program. Evolvable Mach. 22 (1) (2021) 5–33.
[25] A. Garg, P. Aggarwal, Y. Aggarwal, M. Belarbi, H. Chalak, A. Tounsi, R. Gulia, Machine learning models for predicting the compressive strength of concrete containing nano silica, Comput. Concr. 30 (1) (2022) 33–42.
[26] Z. Li, G. Yan, Machine learning for structural stability: predicting dynamics responses using physics-informed neural networks, Comput. Concr. 29 (6) (2022) 419–432.
[27] I. Jeon, T. Yun, S. Yang, Classical, coarse-grained, and reactive molecular dynamics simulations on polymer nanocomposites, Multiscale Science and Engineering (2022) 1–18.
[28] A. Mohammed, R. Kurda, D.J. Armaghani, M. Hasanipanah, Prediction of compressive strength of concrete modified with fly ash: applications of neuro-swarm and neuro-imperialism models, Comput. Concr. 27 (2021) 489–512.
[29] D. Elmo, A. Mitelman, Modeling concrete fracturing using a hybrid finite-discrete element method, Comput. Concr. 27 (4) (2021) 297–304.
[30] S. Sun, R. Ouyang, B. Zhang, T.-Y. Zhang, Data-driven discovery of formulas by symbolic regression, MRS Bull. 44 (7) (2019) 559–564.
[31] M.E. Kotanchek, E.Y. Vladislavleva, G.F. Smits, Symbolic Regression via Genetic Programming as a Discovery Engine: Insights on Outliers and Prototypes, Genetic Programming Theory and Practice VII, Springer, 2010, pp. 55–72.
[32] S.S.M. Astarabadi, M.M. Ebadzadeh, Genetic programming performance prediction and its application for symbolic regression problems, Inf. Sci. 502 (2019) 418–433.
[33] G. Kim, J. Jang, H.R. Khalid, H.-K. Lee, Water purification characteristics of pervious concrete fabricated with CSA cement and bottom ash aggregates, Construct. Build. Mater. 136 (2017) 1–8.
[34] H.-K. Kim, Y. Lim, M. Tafesse, G. Kim, B. Yang, Micromechanics-integrated machine learning approaches to predict the mechanical behaviors of concrete containing crushed clay brick aggregates, Construct. Build. Mater. 317 (2022), 125840.

[35] R.K. Biswas, P. Khan, S. Mukherjee, A.K. Mukhopadhyay, J. Ghosh, K. Muraleedharan, Study of short range structure of amorphous Silica from PDF using Ag radiation in laboratory XRD system, Raman and NEXAFS, J. Non-Cryst. Solids 488 (2018) 1–9.
[36] G. Kim, J.G. Jang, F. Naeem, H.-K. Lee, Heavy metal leaching, CO2 uptake and mechanical characteristics of carbonated porous concrete with alkali-activated slag and bottom ash, International Journal of Concrete Structures and Materials 9 (3) (2015) 283–294.
[37] A. Bahari, M. Ghovati, A. Hashemi, Studying of SiO2/capron nanocomposite as a gate dielectric film for improved threshold voltage, Appl. Phys. A 125 (4) (2019) 1–7.
[38] G. Kim, H. Yoon, H.-K. Lee, Autogenous shrinkage and electrical characteristics of cement pastes and mortars with carbon nanotube and carbon fiber, Construct. Build. Mater. 177 (2018) 428–435.
[39] H. Wang, H. Shin, Recent studies on the multiscale models for predicting fracture toughness of polymer nanocomposites, Multiscale Science and Engineering 4 (2022) 1–9.
[40] J. Cho, S.-K. Lee, S.-H. Eem, J.G. Jang, B. Yang, Enhanced mechanical and thermal properties of carbon fiber-reinforced thermoplastic polyketone composites, Compos. Appl. Sci. Manuf. 126 (2019), 105599.
[41] K. Laoubi, Z. Hamadi, A.A. Benyahia, A. Serier, Z. Azari, Thermal behavior of E-glass fiber-reinforced unsaturated polyester composites, Compos. B Eng. 56 (2014) 520–526.
[42] M.M. Gomaa, C. Hugenschmidt, M. Dickmann, E.E. Abdel-Hady, H.F. Mohamed, M.O. Abdel-Hamed, Crosslinked PVA/SSA proton exchange membranes: correlation between physiochemical properties and free volume determined by positron annihilation spectroscopy, Phys. Chem. Chem. Phys. 20 (44) (2018) 28287–28299.
[43] M. Hartman, O. Trnka, O. Šolcová, Thermal decomposition of aluminum chloride hexahydrate, Ind. Eng. Chem. Res. 44 (17) (2005) 6591–6598.
[44] M. Kayama, H. Nagaoka, T. Niihara, Lunar and martian silica, Minerals 8 (7) (2018) 267.
[45] B. Yang, B. Kim, H.-K. Lee, Micromechanics-based viscoelastic damage model for particle-reinforced polymeric composites, Acta Mech. 223 (6) (2012) 1307–1321.
[46] J. Seo, S. Bae, D. Jang, S. Park, B. Yang, H.-K. Lee, Thermal behavior of alkali-activated fly ash/slag with the addition of an aerogel as an aggregate replacement, Cement Concr. Compos. 106 (2020), 103462.
[47] H. Liu, C. Liu, G. Bai, Y. Wu, C. He, R. Zhang, Y. Wang, Influence of pore defects on the hardened properties of 3D printed concrete with coarse aggregate, Addit. Manuf. 55 (2022), 102843.
[48] J. Bang, J.-H. Bae, J. Jung, B. Yang, A short review of the literature on the multiscale modeling of nanoparticle-reinforced composites, Multiscale Science and Engineering 4 (2022) 94–101.
[49] V. Sounthararajan, K. Srinivasan, A. Sivakumar, Micro filler effects of silica-fume on the setting and hardened properties of concrete, Res. J. Appl. Sci. Eng. Technol. 6 (14) (2013) 2649–2654.
[50] C. Zhuang, Y. Chen, The effect of nano-SiO2 on concrete properties: a review, Nanotechnol. Rev. 8 (1) (2019) 562–572.
[51] H. Li, Z. Xue, H. Liang, Y. Guo, G. Liang, D. Ni, Z. Yang, Influence of defoaming agents on mechanical performances and pore characteristics of Portland cement paste/mortar in presence of EVA dispersible powder, J. Build. Eng. 41 (2021), 102780.
[52] M. Nataraja, Y. Nalanda, Performance of industrial by-products in controlled low-strength materials (CLSM), Waste Manag. 28 (7) (2008) 1168–1181.
[53] M. Gabr, J.J. Bowders, Controlled low-strength material using fly ash and AMD sludge, J. Hazard Mater. 76 (2–3) (2000) 251–263.
[54] J. Yang, W. She, W. Zuo, Q. Zhang, Rational application of nano-SiO2 in cement paste incorporated with silane: counterbalancing and synergistic effects, Cement Concr. Compos. 118 (2021), 103959.